



## Size analysis of single-core magnetic nanoparticles



Frank Ludwig<sup>a,\*</sup>, Christoph Balceris<sup>a</sup>, Thilo Viereck<sup>a</sup>, Oliver Posth<sup>b</sup>, Uwe Steinhoff<sup>b</sup>,  
Helena Gavilan<sup>c</sup>, Rocio Costo<sup>c</sup>, Lunjie Zeng<sup>d</sup>, Eva Olsson<sup>d</sup>, Christian Jonasson<sup>e</sup>,  
Christer Johansson<sup>e</sup>

<sup>a</sup> Institut für Elektrische Messtechnik und Grundlagen der Elektrotechnik, TU Braunschweig, Braunschweig, Germany

<sup>b</sup> Physikalisch-Technische Bundesanstalt, Berlin, Germany

<sup>c</sup> Instituto de Ciencia de Materiales de Madrid, ICMM/CSIC, Madrid, Spain

<sup>d</sup> Department of Applied Physics, Chalmers University of Technology, Göteborg, Sweden

<sup>e</sup> ACREO Swedish ICT AB, Göteborg, Sweden

### ARTICLE INFO

#### Keywords:

Single-core nanoparticles  
Size distribution  
Transmission electron microscopy  
Dynamic light scattering  
Magnetization  
Brownian and Néel relaxation

### ABSTRACT

Single-core iron-oxide nanoparticles with nominal core diameters of 14 nm and 19 nm were analyzed with a variety of non-magnetic and magnetic analysis techniques, including transmission electron microscopy (TEM), dynamic light scattering (DLS), static magnetization vs. magnetic field ( $M$ - $H$ ) measurements, ac susceptibility (ACS) and magnetorelaxometry (MRX). From the experimental data, distributions of core and hydrodynamic sizes are derived. Except for TEM where a number-weighted distribution is directly obtained, models have to be applied in order to determine size distributions from the measurand. It was found that the mean core diameters determined from TEM,  $M$ - $H$ , ACS and MRX measurements agree well although they are based on different models (Langevin function, Brownian and Néel relaxation times). Especially for the sample with large cores, particle interaction effects come into play, causing agglomerates which were detected in DLS, ACS and MRX measurements. We observed that the number and size of agglomerates can be minimized by sufficiently strong diluting the suspension.

### 1. Introduction

There is a wide field of applications of iron oxide magnetic nanoparticles (MNPs) with sizes from a few nm up to several micrometers in biomedical diagnosis, therapy and imaging [1,2]. Central objective of the current research is the standardization of MNP characterization methods [3]. MNPs can be classified into single- and multi-cores [4]. This contribution deals with the analysis of single-core nanoparticles. Single-core MNPs in biomedical applications consist of a single magnetic core, typically magnetite, maghemite or a mixture of both, surrounded by mostly an organic shell. In contrast, multi-core nanoparticles consist of several nanocrystals (magnetic cores) either densely or loosely packed within the multi-core structure and embedded in a matrix [3,4].

There is a variety of analysis methods which can be applied to estimate the core's magnetic moment, its size, anisotropy energy and the hydrodynamic size of the whole particle. Among them are

transmission (TEM) and scanning electron microscopy (SEM), dynamic light scattering (DLS), asymmetrical flow field-flow fractionation (A4F) in combination with light scattering, X-ray and neutron scattering techniques as well as magnetic techniques such as static magnetization vs. magnetic field ( $M$ - $H$ ), ac susceptibility (ACS), magnetorelaxometry (MRX) and magnetic particle spectroscopy (MPS) measurements. Other analysis techniques such as Mössbauer spectroscopy provide information on the elementary composition. Most of the techniques require models to derive one or more of the listed nanoparticle parameters. In addition, since most methods measure the response of an ensemble of MNPs, the quantification of magnetic interactions between particles is an important issue.

In this paper, we summarize the analysis results of single-core iron oxide nanoparticles with nominal core diameters of 14 nm and 19 nm coated with dimercaptosuccinic acid (DMSA) applying static  $M$ - $H$ , ACS vs. frequency, MRX, TEM and DLS measurements. As a consequence of the variety of analysis methods, there is some redundancy in parameters which helps one to verify and refine models.

\* Corresponding author.

E-mail address: [f.ludwig@tu-bs.de](mailto:f.ludwig@tu-bs.de) (F. Ludwig).

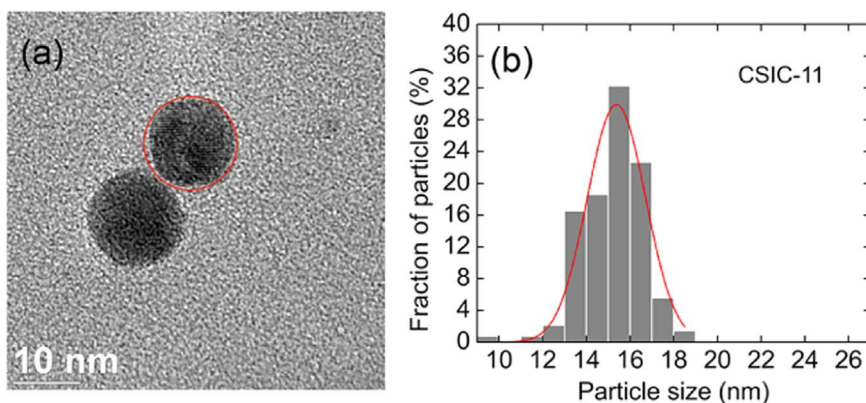


**Fig. 1.** (a) TEM images of individual single-core nanoparticle of CSIC-11. (b) Histogram of core size distribution of 147 particles.

## 2. Experimental

### 2.1. Materials and methods

Both samples, CSIC-11 and CSIC-12, are composed of maghemite/magnetite nanoparticles synthesized by thermal decomposition of iron oleate. The samples were transferred to aqueous media via ligand exchange with DMSA. Details can be found in [5]. An increase in size was obtained by reducing the oleic acid content in the reaction media.

Measurements were mostly carried out in suspensions. In some cases, samples with MNP immobilized by freeze-drying were studied. Iron contents of samples were determined by inductively coupled plasma-optical emission spectrometry (ICP-OES, PerkinElmer Optima 2100 DV ICP) after dissolving the samples in  $\text{HNO}_3:\text{HCl}$  1:3 mixtures and diluting them with doubly distilled water.

Static magnetization measurements were performed with a Magnetic Property Measurement System (MPMS-XL, Quantum Design).

ACS vs. frequency measurements were carried out with different setups: The commercially available DynoMag system from Acreo which operates in a frequency range from 1 Hz to 500 kHz as well as custom-built systems at Acreo (up to 10 MHz) and the TU Braunschweig systems covering a frequency range from 2 Hz to 1 MHz. All systems were calibrated with  $\text{Dy}_2\text{O}_3$  powder samples.

MRX measurements were performed with a fluxgate-based system at TU Braunschweig. The relaxation signal was recorded after applying a magnetizing pulse of 2 mT magnitude and 2 s duration. As a consequence of the finite switch-off time of the magnetic field and the bandwidth of the utilized fluxgate sensors of 3 kHz, characteristic relaxation times below about 300  $\mu\text{s}$  are not accessible.

TEM images were acquired with a FEI Tecnai F20 equipped with a  $\text{LaB}_6$  electron gun and operated at 200 kV. The system was calibrated

from  $\mu\text{m}$  to atomic scale by using a standard TEM cross grating sample (Au nanoparticles on amorphous C film).

A Malvern Zetasizer Nano ZS was used for DLS measurements. The autocorrelation function was recorded in the  $173^\circ$  backscatter mode. The data analysis was performed either with the 2nd cumulant method or the general-purpose model (nonlinear-non-negative least square (NNLS) method).

### 2.2. Experimental results

In Fig. 1(a), a TEM image of samples CSIC-11 is shown. The MNPs of CSIC-11 were found to be octahedral, which is a consequence of the synthesis process [5], and 70% of the 147 analyzed particles are single-core; the remaining 30% occur in the form of small agglomerates. The histogram of core diameters – assuming spherical shape – is depicted in Fig. 1(b). The arithmetic mean diameter amounts to  $(14.1 \pm 1.3)$  nm. A TEM image of CSIC-12 is shown in Fig. 2(a). Analyzing a total of 187 particles, it was found that they have a truncated octahedral shape (h/w ratio of 1.2) and that about 85% of them are present as isolated single-core particles. The arithmetic mean core diameter was determined as  $(21 \pm 3)$  nm.

DLS measurements on suspensions with 0.1 mg(Fe)/mL – applying the 2nd cumulant method – provided Z-averages of 25 nm and 46 nm as well as polydispersity indices (PDI) of 0.21 and 0.35 for CSIC-11 and CSIC-12 suspensions, respectively. Assuming a lognormal distribution of hydrodynamic diameters, number-weighted mean diameters of 14 nm and 25 nm were calculated. Fig. 3 shows the intensity-, volume- and number-weighted distributions of hydrodynamic diameters of CSIC-12 obtained by applying the NNLS method on the analysis of the autocorrelation function. Apparently, there is a second peak at hydrodynamic diameters between 100 nm and 300 nm which is most pronounced in the intensity-weighted distribution. This second peak is

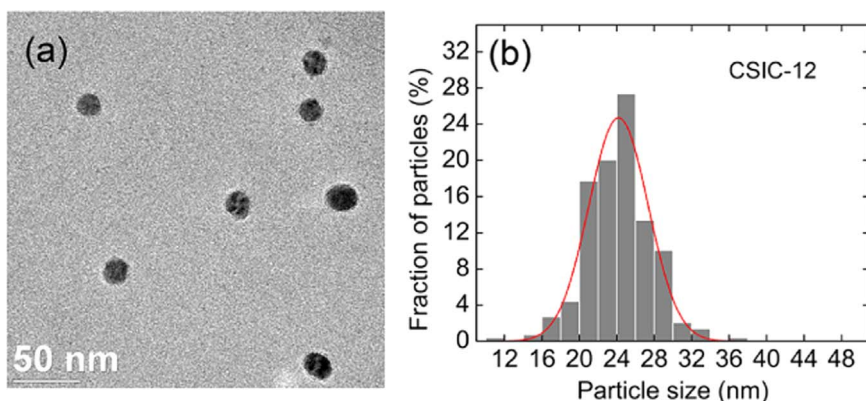


**Fig. 2.** (a) TEM image of CSIC-12. (b) Histogram of core size of 187 particles.

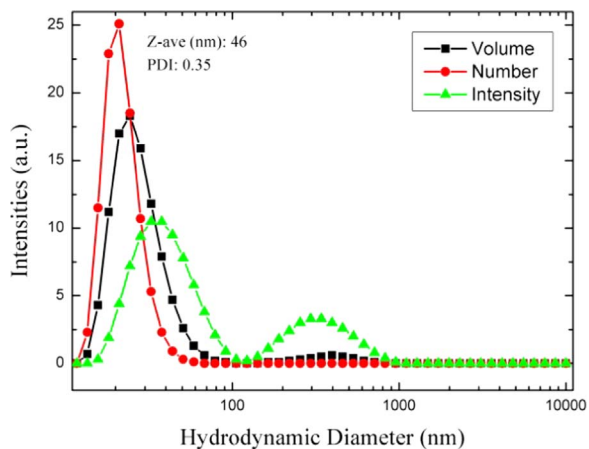


**Fig. 3.** Intensity-, volume- and number-weighted distribution of hydrodynamic diameters of CSIC-12 (0.1 mg(Fe)/mL) obtained from the NNLS analysis of DLS data.

attributed to agglomerates. Due to the weighting of the DLS signal proportional to the nanoparticle volume squared, this maximum is not discernable in the number-weighted distribution. Whereas the maximum at around 30 nm in the intensity-weighted distribution is the same for the explored dilutions, thus originating from light scattering on individual single-core nanoparticles, both the amplitude and the position of the second maximum were found to depend on MNP concentration and pH value of the suspension. The presence of larger agglomerates presumably explains the difference in polydispersity between TEM and DLS data.

Fig. 4 depicts the static  $M$ - $H$  curves measured at 300 K on CSIC-11 and CSIC-12 suspensions. Although the measured signal was corrected for that measured on an empty sample container, there remains a tiny residual slope at large magnetic fields (CSIC-11:  $1.75 \cdot 10^{-6}$  m<sup>3</sup>/kg; CSIC-12:  $1.6 \cdot 10^{-6}$  m<sup>3</sup>/kg). This effect can be ascribed to the spin arrangement at the particle surface where very high fields are needed to saturate the surface spins [6] and it is supported by the fact that the slope for the larger CSIC-12 MNPs is slightly smaller than for CSIC-11. Since the saturation field is unknown where all spins are aligned in field direction, we determined the saturation mass magnetization from the measured magnetic moment of the sample at the largest field (4.9 T) and the determined Fe content of the sample. For CSIC-11 and CSIC-12 it amounts to 118(3) A·m<sup>2</sup>/kg<sub>Fe</sub> and 128(3) A·m<sup>2</sup>/kg<sub>Fe</sub>, respectively. This reaches almost the value of bulk magnetite (130 A·m<sup>2</sup>/kg<sub>Fe</sub> [7]). Thus we assume the core material to be magnetite with an iron density of 3763 kg<sub>Fe</sub>/m<sup>3</sup> and a resulting saturation magnetization  $M_s$  of the CSIC-11 core material of 444 kA/m; for CSIC-12  $M_s$  equals 482 kA/m.

The measured curves were fitted with the Langevin function extended by a lognormal distribution of core volumes  $f(V_c, \bar{V}, \sigma_c)$ —assuming that all MNP have the same saturation magnetization  $M_s$  [8]:

$$M(H, T) = \frac{1}{V \cdot c_{Fe}} \int_0^{V_{max}} f(V_c, \bar{V}, \sigma_c) \cdot m(V_c) \cdot L(V_c, H, T) dV_c$$

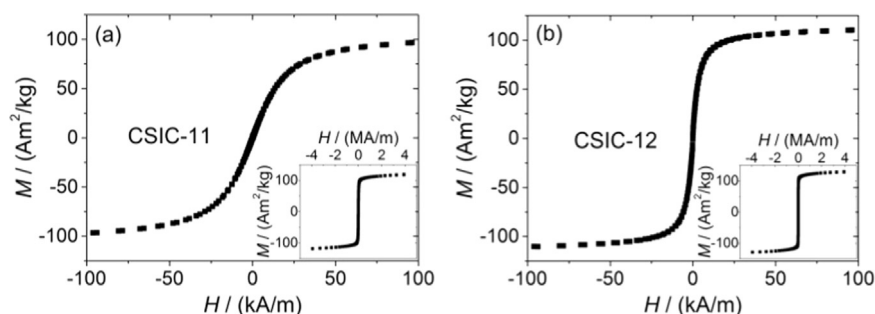


**Fig. 4.** Mass magnetization vs. magnetic field ( $M$ - $H$ ) curves of (a) CSIC-11 and (b) CSIC-12 suspensions at 300 K. Inset: Larger magnetization field up to 3.9 MA/m.

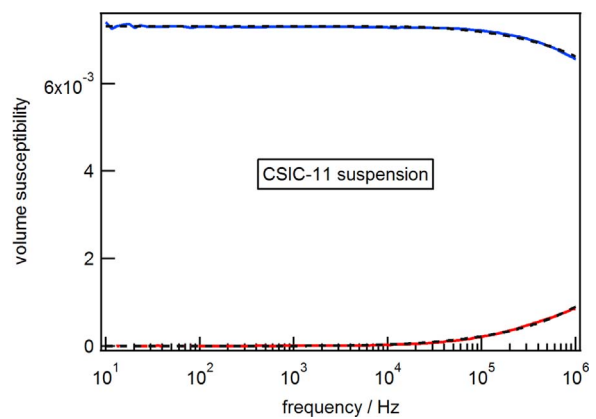


**Fig. 5.** Real and imaginary part of ac susceptibility measured on CSIC-11 suspension. Solid lines show experiment, dashed ones fit with extended Debye model.

Here  $m(V_c) = M_s V_c$  is the magnetic moment of a single MNP with an effective core volume  $V_c$ , and  $L(V_c, H, T)$  is the Langevin function. The measured  $M$ - $H$  curves could be well fitted for both samples with a single lognormal distribution of core volumes. Assuming spherical cores, arithmetic mean diameters and standard deviations of 12.3 nm and 1.1 nm were determined for CSIC-11 whereas 17.6 nm and 4.5 nm were found for CSIC-12. It has to be noted that model deviations in terms of  $M_s$ , core material and core anisotropy will all have an influence on the size distribution that is estimated from  $M$ - $H$  curves.

Real and imaginary parts of the ac susceptibility measured on the CSIC-11 suspension are depicted in Fig. 5. Basically the same spectra were measured on a freeze-dried reference sample, indicating that the dynamics are dominated by the internal Néel mechanism. Therefore, no information on the hydrodynamic nanoparticle size can be obtained from the ACS analysis. However, replacing  $\tau_{eff}$  in Eq. (2) with the Néel relaxation time

$$\tau_N = \tau_0 \exp \left[ \frac{KV_c}{k_B T} \right] \quad (1)$$

and assuming  $\tau_0 = 10^{-10}$  s, a median core diameter of about 10 nm is estimated from fitting the model to the measured susceptibility spectra. For the anisotropy constant  $K$ , a value of about 22 kJ/m<sup>3</sup> is found. It should be noted that the accuracy of these parameters is not very high since the relaxation maximum is outside the measurement window and the Néel relaxation time provides a measure of the anisotropy energy, i.e., the product of  $K$  and  $V_c$ .

Fig. 6 shows real and imaginary parts measured on CSIC-12 suspensions with varying Fe content (i.e. varying MNP concentration). Apparently, at high iron concentrations, a second relaxation maximum in the imaginary part evolved below 10 Hz (see Fig. 6). Both relaxation maxima are caused by Brownian rotation: the maximum at around 30 kHz by that of individual MNPs and the one below 10 Hz by that of particle agglomerates. With increasing dilution the latter relaxation maximum gradually vanishes. Since the volume susceptibility is

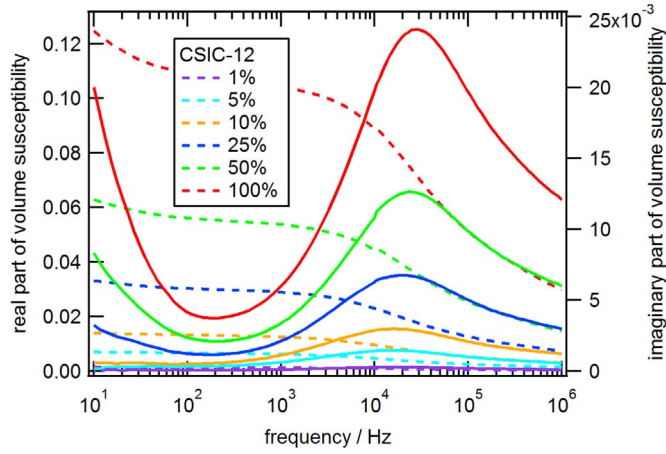


Fig. 6. Real and imaginary part of ac susceptibility measured on different volume dilutions of CSIC-12 suspension.

plotted, the maximum at around 30 kHz also decreases with increasing volume dilution. Since a significant portion of particles contributes to the low-frequency maximum at high concentrations, the scaling of the amplitude of the maximum, which is attributed to the Brownian rotation of single-core nanoparticles, with the Fe concentration is not strictly linear.

To fit the measured spectra, a generalized Debye model is applied [9,10]. Then the complex susceptibility is given by

$$\chi(\omega) = \chi_0^{**} \int_0^\infty f(d_h) \int_0^\infty d_c^6 f(d_c) \frac{1}{1 + i\omega\tau_{eff}} dd_c dd_h + \chi_\infty \quad (2)$$

$$\text{with } \chi_0^{**} = \frac{\mu_0 n M_c^2}{3k_B T} \langle V_c \rangle^2.$$

Here the effective relaxation time is given by  $\tau_{eff} = \tau_B \tau_N / (\tau_B + \tau_N)$  with the Brownian relaxation time

$$\tau_B = \frac{3\eta V_h}{k_B T}.$$

Furthermore,  $\omega = 2\pi f$  is the angular frequency,  $\chi_\infty$  the susceptibility at high frequencies,  $n$  the concentration of MNP,  $\langle V_c \rangle$  the mean core volume,  $V_h$  the hydrodynamic volume, and  $T$  the thermodynamic temperature. For the distributions of core diameters  $f(d_c)$  and hydrodynamic diameters  $f(d_h)$  lognormal functions are assumed:

$$f(d_{c,h}) = \frac{1}{\sqrt{2\pi} \sigma_{c,h} d_{c,h}} \exp\left[-\frac{(\ln(d_{c,h}) - \mu)^2}{2\sigma_{c,h}^2}\right]$$

with  $\mu$  and  $\sigma$  being mean and standard deviation of the diameter's

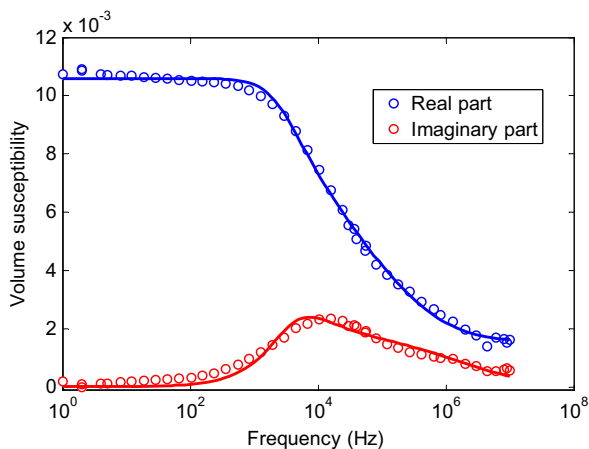


Fig. 7. Real and imaginary part of CSIC-12 suspension with 0.51 mg(Fe)/mL. Solid lines show best fit with Eq. (4).

natural logarithm. Indices “c” and “h” stand for core and hydrodynamic, respectively. The analysis of ACS data with Eq. (2) contains information on the hydrodynamic size distribution  $f(d_h)$  (via the Brownian relaxation time  $\tau_B$ ) and the core size distribution  $f(d_c)$  (via the Néel relaxation time  $\tau_N$ ). To limit the number of free parameters, it is recommended to determine the core parameters  $\mu_c$ ,  $\sigma_c$ , and  $K$  from ACS or MRX measurements on an immobilized sample.

If the MNP magnetic moments are thermally blocked, all MNP follow the applied ac magnetic field via the Brownian mechanism. Then Eq. (1) simplifies to

$$\chi(\omega) = \chi_0^{**} \int_0^\infty f(d_h) \frac{1}{1 + i\omega\tau_B} dd_h + \chi_\infty \quad (3)$$

Fitting the susceptibility spectra of the CSIC-12 suspension with 0.79 mg(Fe)/mL with Eq. (3) provides a hydrodynamic diameter of  $(29.5 \pm 3.5)$  nm. Including Néel relaxation (Eq. (2)), a slightly larger value  $(37.6 \pm 5.1)$  nm is obtained.

Replacing the hydrodynamic diameter  $d_h$  by  $d_h = d_c + 2d_{sh}$  with shell thickness  $d_{sh}$ , Eq. (2) modifies for spherical particles to

$$\chi(\omega) = \chi_0^* \int_0^\infty d_c^6 f(d_c) \frac{1}{1 + i\omega\tau_{eff}} dd_c + \chi_\infty \quad (4)$$

$$\text{with } \chi_0^* = \frac{\mu_0 n M_c^2}{3k_B T} \left(\frac{\pi}{6}\right)^2, \quad n = \frac{c_{Fe}\epsilon}{\rho \langle V_c \rangle}$$

$$\text{and } \tau_B = \frac{\pi(d_c + 2d_{sh})^3}{2k_B T}.$$

Here,  $c_{Fe}$  is the iron concentration in the sample,  $\rho$  the density of iron-oxide in the magnetic core, and  $\epsilon$  is a mass conversion factor between iron and the actual iron-oxide in the core. Thus, including the calibrated AC susceptibility of the sample in the fitting procedure provides a method of determining the core diameter, shell thickness and magnetic anisotropy constant  $K$  (via the Néel relaxation time in  $\tau_{eff}$ ).

Fig. 7 depicts the susceptibility spectra measured on a diluted CSIC-12 suspension (0.51 mg(Fe)/mL) and the best fit with Eq. (4). The following parameters were obtained: a median core diameter (number-weighted) of 19.4 nm, a shell thickness of 8 nm and an anisotropy constant  $K = 11$  kJ/m<sup>3</sup>. As can be seen in Fig. 7 there is some discrepancies from the fitting result and data at low frequencies below 1 kHz. This is due to that the MNP system has a low frequency process (even if the system is diluted) and the model in Eq. (4) does not take this into account. The low frequency relaxation can be seen as a non-zero imaginary part and a slope in the real part at lower frequencies (see Fig. 7).

To fit the susceptibility spectra measured on more concentrated samples, a bimodal distribution of hydrodynamic and core diameters can be implemented in Eqs. (2)–(4), respectively.

MRX measurements on CSIC-11, either on suspended or on immobilized particles, show a very fast decay of the relaxation signal with a characteristic time outside the measurement window. This finding is consistent with the ACS results which indicated that characteristic frequencies are well above 1 MHz. Fig. 8 shows the relaxation curves measured on a suspension and a freeze-dried CSIC-12 sample, each having a concentration of 0.79 mg(Fe)/mL.

The MRX curves can be described by the moment superposition model assuming non-interacting nanoparticles [11–13]. Here the decay of the effective magnetic moment of the sample can be described by

$$m_r(t) = M_s \int_0^\infty f(V_c) \cdot V_c \cdot L(V_c, H) \times \left[ 1 - \exp\left(-\frac{t_{mag}}{\tau_{N,H}}\right) \right] \exp\left(-\frac{t}{\tau_N}\right) dV_c \quad (5)$$

for immobilized particles and by

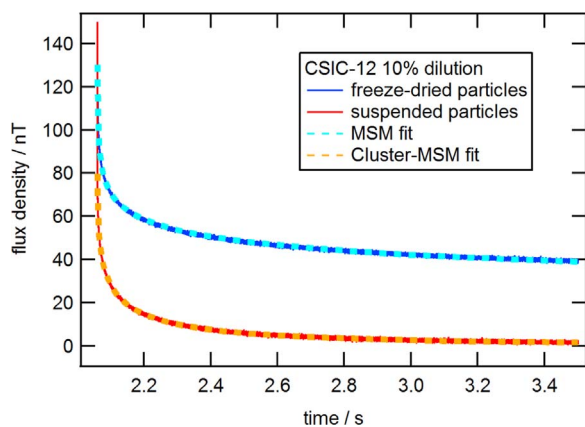


**Fig. 8.** MRX curves measured on suspended and immobilized CSIC-12 sample with 0.79 mg(Fe)/mL along with best fits with Eqs. (5) and (6) respectively.

$$m_r(t) = M_s \int_0^\infty f(d_h) \int_0^\infty f(V_c) \cdot V_c \cdot L(V_c, H) \times \left[ 1 - \exp\left(-\frac{t_{\text{mag}}}{\tau_{\text{eff},H}}\right) \right] \exp\left(-\frac{t}{\tau_{\text{eff}}}\right) dV_c dV_h \quad (6)$$

for suspended ones. Here the subscript “H” denotes that this is the corresponding relaxation time in the presence of the magnetizing field. For  $f(d_h)$  and  $f(d_c)$  lognormal distributions are assumed. For the Néel relaxation time in zero magnetic field, Eq. (1) is used with  $\tau_0 = 1$  ns. Since in Eq. (6) for fitting MRX curves on MNP suspensions Brownian and Néel relaxation must be considered, it is recommended to first fit the relaxation curve measured on an immobilized sample with Eq. (5), thus determining the core size distribution parameters and anisotropy constant, and then to fit the relaxation curve for the suspended MNP.

As can be seen in Fig. 8, the measured curves can be very well fitted with Eqs. (5) and (6). The determined MNP parameters are the following: core diameter ( $20.0 \pm 5.9$ ) nm, hydrodynamic diameter ( $732 \pm 620$ ) nm (standard deviation of logarithm of hydrodynamic diameter  $\sigma_h = 0.74$ ). Additionally, from fitting the MRX curve measured on the immobilized sample, an effective anisotropy constant  $K = 12$  kJ/m<sup>3</sup> was obtained, in excellent agreement with the value from the ACS analysis.

### 3. Discussion

The size distribution parameters determined for CSIC-12 are summarized in Table 1. As can be seen there is quite good consistency in the core size parameters. Whereas the TEM data are obtained without applying models, all magnetic methods require physical models. The analysis of  $M-H$ , ACS, MRX and DLS data is based on the assumption of lognormal distributions of diameters (assuming spherical particles). The core size estimated from static  $M-H$  measurements relies on the Langevin function, thus primarily estimating the

**Table 1**

Derived MNP parameters from various analysis techniques on suspended and immobilized particles of CSIC-12.  $d_c$  and  $d_h$  are arithmetic mean core and hydrodynamic diameters, respectively, and  $\sigma_c$  and  $\sigma_h$  are the corresponding standard deviations. Values in brackets are caused by particle agglomerates/clusters.

	TEM	DLS	$M-H$	ACS	MRX
$d_c$ / nm	21		17.6	19.4	20.0
$\sigma_c$ / nm	3		4.5	2.5	5.9
$d_h$ / nm		25.0		29.5 (Eq. (3)) 35.4 (Eq. (4))	
		( $\approx 150$ )		( $\approx 650$ )	( $\approx 730$ )
$\sigma_h$ / nm				3.5 (Eq. (3))	( $\approx 620$ )

distribution of magnetic moments  $f(m)$ . Knowing the saturation magnetization which can be estimated from the measured magnetic moment of the sample at high applied magnetic fields and from the determined Fe content, the distribution of magnetic core volumes can be calculated. The core diameter as estimated by applying Eq. (2) to analyze the ACS spectra also relies on the knowledge of the Fe content which determines the static susceptibility  $\chi_0$ . In addition, this analysis provides the effective thickness of the MNP shell.

The analysis of ACS spectra measured on suspended thermally blocked nanoparticles with Eq. (1) directly provides the distribution of hydrodynamic size, proposed that the dynamic viscosity is known. There is some scatter in the mean hydrodynamic diameter obtained from DLS, ACS and MRX measurements. In MRX – as a consequence of the restricted measurement window – the measurable decay is dominated by agglomerates/clusters, i.e., the signal decay caused by the single-core nanoparticles is too fast. Interestingly, the mean hydrodynamic size of agglomerates is comparable to that estimated from ACS spectra but much larger than that from DLS measurements. One possible explanation might be that the presence of the 2 mT magnetizing magnetic field in MRX and the sinusoidal excitation magnetic field in ACS strengthen the agglomeration.

As shown in Figs. 3 and 6, the contribution of agglomerates depends on MNP concentration. With increasing dilution the mean size and number of agglomerates decrease, e.g., causing a vanishing of the low-frequency maximum in the ACS imaginary part. This particle interaction is much weaker for CSIC-11 as a consequence of the smaller magnetic moments/core sizes. Due to the comparably small core size, the Néel relaxation time of these single-core nanoparticles is shorter than the Brownian relaxation time, so that the magnetic dynamics are dominated by the internal Néel mechanism. Therefore, neither ACS nor MRX measurements using the current setups provide information on their hydrodynamic size.

One important difference between analysis techniques is their different weighting by the particle and/or core size. Whereas TEM directly provides a number-weighted core size distribution, the DLS signal is weighted by intensity, i.e., by the hydrodynamic volume squared. Thus, converting the intensity-weighted size distribution into a number-weighted one, can cause quite large errors (as can be seen in Fig. 3). The net magnetic moment of the whole sample in  $M-H$  and MRX measurements is the sum of single particle magnetic moments  $m$ , i.e., the curve directly reflects a volume-weighted moment distribution. If all MNPs in a suspension are thermally blocked, the analysis of the ACS spectrum directly provides a number-weighted distribution of hydrodynamic size. In contrast, for Néel relaxation dominated nanoparticles as well as by applying Eq. (4) for the analysis of ACS spectra measured on suspended MNP, the number-weighted distribution is weighted with the core volume squared, resulting – similarly to DLS – in a volume weighted core size distribution.

### 4. Conclusions

We determined the distribution of core and hydrodynamic diameters of single-core iron oxide nanoparticle samples with nominal core diameters of 14 nm and 19 nm applying different non-magnetic and magnetic analysis techniques. TEM, static  $M-H$ , ACS and MRX measurements provided roughly the same core diameter for CSIC-12 although the determination of the core size from the respective measurand is based on different models:

- in TEM a number-weighted distribution is directly obtained by plotting the diameters of a sufficiently large number single nanoparticles into a histogram
- static  $M-H$  curves provide the distribution of magnetic moments by applying the Langevin function
- a novel model to analyze the ac susceptibility spectra measured on suspensions provides the core diameter via the estimation of the

Brownian relaxation time and the analysis of the static susceptibility – MRX measurements on immobilized MNP provide a distribution of Néel relaxation times which depend on the core volume

Interestingly, the mean core diameter determined from  $M$ - $H$  measurements was found to be somewhat smaller than the values obtained from the other analysis techniques.

For CSIC-11, having a mean core diameter of 14 nm, the dynamics are dominated by the internal Néel mechanism so that no information on the hydrodynamic size via the Brownian relaxation time is contained in dynamic magnetic measurements. The Néel relaxation time is found to be well below 1  $\mu$ s, i.e., outside the measurement window of the utilized ACS and MRX systems.

Since the determined hydrodynamic diameters from DLS and ACS are close to the determined magnetic core diameters from  $M$ - $H$ , MRX and ACS analysis, we conclude that the investigated MNP systems are single-core MNP systems.

For concentrated suspensions of CSIC-12, a bimodal distribution of hydrodynamic sizes was found in ACS, MRX and DLS measurements. This contribution was found to diminish if the suspension was sufficiently diluted. The hydrodynamic diameters of individual single-core nanoparticles estimated from DLS and ACS measurements were found to be in fair agreement.

The findings presented in this paper were supported by other measurement techniques (not shown here) and represent an important step towards a standardization of the analysis of magnetic nanoparticles. The good agreement of structural properties determined by different magnetic and nonmagnetic methods proves the applicability of these techniques and their related models for the characterization of single-core nanoparticles.

## Acknowledgements

This work was supported by the European Commission Framework

Programme 7 under the NanoMag project (grant agreement no: 604448).

## References

- [1] Q.A. Pankhurst, N.T.K. Thanh, S.K. Jones, J. Dobson, Progress in applications of magnetic nanoparticles in biomedicine, *J. Phys. D Appl. Phys.* D 42 (2009) 224001.
- [2] K.M. Krishnan, Biomedical nanomagnetism: a *spin* through possibilities in imaging diagnostics, and therapy, *IEEE Trans. Magn.* 46 (2010) 2523.
- [3] O. Posth, M.F. Hansen, U. Steinhoff, L. Bogart, P. Southern, P. Svedlindh, C. Grüttner, L. Fernández Barquin, W. Szczerba, F. Ludwig, N. Gehrke, O. Kazakova, C. Johansson, Classification of analysis methods for characterization of magnetic nanoparticles, XXI IMEKOWorld Congress Measurement in Research and Industry, Prague, Czech Republic, 2015.
- [4] S. Bogren, A. Fornara, F. Ludwig, M.P. Morales, U. Steinhoff, M.F. Hansen, O. Kazakova, C. Johansson, Classification of magnetic nanoparticle systems—synthesis, standardization and analysis methods in the NanoMag project, *Int. J. Mol. Sci.* 16 (2015) 20308.
- [5] G. Salas, C. Casado, F. Teran, R. Miranda, C.J. Serna, M.P. Morales, Controlled synthesis of uniform magnetite nanocrystals with high-quality properties for biomedical applications, *J. Mater. Chem.* 22 (2012) 21065.
- [6] X. Batlle, A. Labarta, Finite-size effects in fine particles: magnetic and transport properties, *J. Phys. D Appl. Phys.* 35 (6) (2002) R15.
- [7] R.C. O'Handley, *Modern magnetic materials: principles and applications*, Wiley, New York, 2000.
- [8] D. Eberbeck, F. Wiekhorst, S. Wagner, L. Trahms, How the size distribution of magnetic nanoparticles determines their magnetic particle imaging performance, *Appl. Phys. Lett.* 98 (2011) 182502.
- [9] S.-H. Chung, A. Hoffman, K. Guslienko, S.D. Bader, C. Lui, B. Kay, L. Makowski, L. Chen, Biological sensing with magnetic nanoparticles using Brownian relaxation, *J. Appl. Phys.* 97 (2005) 10R101.
- [10] F. Ludwig, Characterization of magnetic core-shell nanoparticle suspensions using ac susceptibility for frequencies up to 1 MHz, *AIP Conf. Proc.* 1311 (2010) 249.
- [11] R.W. Chantrell, S.R. Hoon, B.K. Tanner, Time-dependent magnetization in fine-particle ferromagnetic systems, *J. Magn. Magn. Mater.* 38 (1983) 133.
- [12] D. Eberbeck, F. Wiekhorst, U. Steinhoff, L. Trahms, Aggregation behaviour of magnetic nanoparticle suspensions investigated by magnetorelaxometry, *J. Phys. Condens. Matter* 18 (2006) S2829.
- [13] F. Ludwig, E. Heim, M. Schilling, K. Enpuku, Characterization of superparamagnetic  $\text{Fe}_3\text{O}_4$  nanoparticles by fluxgate magnetorelaxometry for use in biomedical applications, *J. Appl. Phys.* 103 (2008) 07A314.